

ISTITUTO NAZIONALE DI FISICA NUCLEARE

INFN/BE - 70/6

18 Settembre 1970

U. Abbondanno, R. Giacomich, L. Granata, M. Lagonegro and G. Pauli:

**DESCRIPTION OF AN EXPERIMENTAL ARRANGEMENT FOR STUDYING THE
GAMMA RAYS RESULTING FROM INTERACTION OF 14.2 MeV NEUTRONS
WITH VARIOUS ELEMENTS**

DESCRIPTION OF AN EXPERIMENTAL ARRANGEMENT FOR STUDYING THE
GAMMA RAYS RESULTING FROM INTERACTIONS OF 14.2 MeV NEUTRONS
WITH VARIOUS ELEMENTS

U. Abbondanno, R. Giacomich, L. Granata, M. Lagonegro and
G. Pauli

Istituto di Fisica, Università di Trieste, Italia
Istituto Nazionale di Fisica Nucleare, Sottosezione di Trieste, Italia

1. - INTRODUCTION

During the period from January 1969 to March 1970 the 600 keV Cockcroft - Walton accelerator of the Istituto di Fisica di Trieste has been utilized to carry out measurements concerning the γ -rays produced in the interaction of neutrons having an energy of about 14 MeV with various target nuclei.

The apparatus employed in these measurements combines the techniques of particle time-of-flight spectroscopy and γ -ray spectroscopy.

The purpose of this report is to describe the experimental set-up and to discuss its principal performances.

2. - EXPERIMENTAL APPARATUS AND TECHNIQUES

A schematic diagram of the experimental arrangement is shown in Fig. 1.

The neutrons are produced with the $T(d,n)^4He$ reaction by bombarding a tritiated titanium target with a $\sim 5 \mu A$ beam of 200 keV deuterons from the Cockcroft-Walton accelerator.

The α -particles produced in the reaction, simultaneously with the neutrons which will be called in the following "associated neutrons", are detected at 90° with respect to the deuteron beam direction by means of a NE 810 α -particle detector (a plastic scintillator 0.03" thick mounted on a light pipe 0.1" thick) coupled with a 56 AVP photomultiplier. A diaphragm placed in front of the scintillator fixed a solid angle, having a half width equal to $5^\circ 20'$, in which the α -particles are counted.

The "associated neutrons" emerge with an energy of 14.200 ± 0.160 MeV in a well defined cone (¹), having a half width equal to $8^\circ 30'$ and the axis at 85° with respect to the dueteron beam.

The scattering sample of cylindrical shape is placed within the cone of the associated neutrons at a distance of 28 cm from the neutron-producing target.

The γ -rays produced by the interaction of the incident neutrons with the scattering sample are detected by means of two 3" \times 3" NaI(Tl) crystals, coupled with XP 1021 photomultipliers, placed at 1 meter from the scattering sample along directions forming supplementary angles with respect to the axis of the cone of the incident neutrons. Both detectors are surrounded by large lead shields. Lead shadow-bars, 50 cm long, are mounted between the target and the gamma counters to reduce the flux of neutrons going directly from the target to the counters.

The discrimination between gamma rays and scattered neutrons going into the NaI(Tl) crystals is performed by means of the time-of-flight method.

The electronics is schematically shown in Fig. 2. A "fast channel" and a "slow channel" can be separately described.

Fast channel. The anode pulses from the XP 1021 photomultipliers are put directly into an active mixer circuit (Fig. 3) having the function of equalizing the input pulses in amplitude and shape. The output signal of the mixer circuit is shaped by a tunnel diode discriminator (Fig. 4) which has an adjustable dead time in order to paralyze the circuit itself for a length of time equal to the input pulse duration. This is of about one microsecond in the case of a NaI(Tl) detector.

The output pulse of the tunnel diode trigger circuit is delayed in order that it is fed into the "start" side of the time-to-pulse-height converter in coincidence with the pulse which gates the converter itself (see below). Before being put into the converter, the start pulse is restored by a second tunnel diode trigger circuit.

The anode pulse from the α -detector is conveniently delayed and shaped and then put into the "stop" side of the time-to-pulse-height converter.

The time inversion of the start and stop signals is required by reasons of counting rate.

Slow channel. It furnishes the pulse to the gate of the time-to-pulse-height converter. This pulse is provided by either of two slow coincidence circuits, one for each γ -detector. Each coincidence circuit

is operated by the diode pulses (shaped by tunnel diode discriminators (Fig. 5)) of the α -detector and of one NaI(Tl) detector. The slow coincidence circuits (Fig. 6) have a variable resolving time ranging from 0.1 μ sec to 0.5 μ sec.

The time-to-pulse-height converter allows to determine the time spectrum between the occurrence of a pulse of the α -detector and a pulse of the NaI(Tl) detectors. On a time scale, one has a narrow peak due to the γ -rays emitted by the scattering sample, followed by a broader peak corresponding to the neutrons scattered by the sample. A single channel analyzer selects the γ -peak and operates the gate of a multichannel analyzer, enabling the analysis of the linear signal of the γ -detectors. Fig. 7 shows the time spectrum obtained for sodium which illustrates the features discussed above.

The linear signal of each γ -detector, taken from the dynode of the photomultiplier, is fed to a chain made up of a preamplifier (Fig. 8), a mixer circuit, a linear amplifier and a delay amplifier and finally is displayed on a 1024 - channel "Laben" analyser. The analysis of the outputs of the two γ -detectors is performed by using two memory subgroups of 512 channels of the analyser. The subgroup selection unit of the analyser is operated by the output pulses of one of the coincidence circuits mentioned above, as illustrated in Fig. 2. The γ -spectra obtained from a sodium sample are shown in Figures 9 and 10.

3. - CHARACTERISTICS OF THE EXPERIMENTAL APPARATUS

The variation with gamma energy of the efficiencies of the NaI(Tl) detectors was required for the determination of the absolute production cross-section of the γ -rays resulting from the neutron inelastic scattering by the samples.

Since the gamma yield could be estimated from the full energy peak of the gamma spectra, the photopeak efficiency was needed. This was obtained by using a set of standard sources of ^{22}Na , ^{137}Cs , ^{207}Bi and ^{88}Y placed at the same position as were the scattering samples during the

measurements. These sources cover the energy range from 0.511 MeV to 1.836 MeV. A further point at 4.43 MeV has been obtained by measuring the production at 90° of the 4.43 MeV γ -rays emitted in the inelastic scattering of 14.2 MeV neutrons from ^{12}C and using the cross-section values reported in ref. (2).

The experimental values of the quantity $\epsilon_p \Delta\Omega$ for both the NaI(Tl) crystals versus the γ -ray energy E_γ , is shown in Fig. 11. ϵ_p is the photopeak efficiency and $\Delta\Omega$ is the solid angle subtended by the detector at the γ -source position.

The γ -spectra measurements have been carried out with the biases of the fast and slow γ -channels set at about 60 keV and 250 keV, respectively.

The overall time resolution of the time of flight apparatus, corresponding to a gamma ray energy greater than 250 keV and to an energy range of nearly 12 MeV, was of about 6 nsec while the window placed over the γ -peak by the single-channel analyser was as large as ~ 15 nsec. The time separation between scattered neutrons and gamma rays was varying with the mass number of the target nuclei and with the angle of observation and had a mean value of 18 nsec. Therefore the neutron contribution affecting the γ -peak was to be expected almost negligible. This point was checked by performing measurements with a ^6Li sample.

4. - MEASUREMENTS

The apparatus has been employed for measuring the angular distributions and the absolute production cross-sections of γ -rays following the inelastic scattering of 14.2 MeV neutrons by various nuclei. Preliminary results are reported in ref. (3).

The scattering samples were in the form of right cylinders and the target materials were of natural isotopic mixture. The samples made of powder were enclosed in thin perspex cylindrical containers.

No correction has been made to take the absorption and the multi-

ple scattering of neutrons in the samples into account, since these effects were assumed to balance each other. This point has been checked by performing measurements with samples of different sizes. The cross-sections thus obtained did not differ from each other by amounts larger than the experimental errors.

A correction for the γ -ray loss, due to the absorption in the scattering sample, has been taken into account and it has been either calculated by using the values of the absorption coefficients tabulated in ref. (4), or measured by means of the γ -ray reference sources.

The background contaminating the measured γ -spectra has been studied by performing measurements with a ${}^6\text{Li}$ sample and with the sample removed. The background spectra showed a smooth shape over the entire energy range of observation, exhibiting only a weak peak due to the annihilation radiation. Fig. 12 shows a typical background spectrum obtained with the sample removed and for an integrated neutron flux of the same magnitude as that usually chosen for the γ -spectra measurements.

The absolute values of the differential production cross-sections of the γ -rays have been deduced by using the formula

$$\left(\frac{\Delta\sigma}{\Delta\Omega}\right)_\vartheta = \frac{N_\gamma(\vartheta) [S(\mu, \langle L \rangle)]^{-1}}{p_A p_n N_n \frac{\rho N}{A} \langle L \rangle \epsilon_p \Delta\Omega}$$

where $N_\gamma(\vartheta)$ = area under the photopeak of the γ -ray spectrum taken at the angle ϑ ,

μ = absorption coefficient of the γ -ray in the scattering sample (cm^{-1}),

$\langle L \rangle$ = mean path in the scattering sample (cm),

p_A = fraction of the target nucleus contained in the sample,

p_n = fraction of the neutrons emitted in the associated neutron cone that impinge upon the sample (for the samples used in the experiments p_n varies from 0.8 and 1.0),

N_n = integral value of the associated neutron flux,

- ρ = density of the scattering material (gr/cm³),
 A = mass number of the target nucleus,
 \mathcal{N} = Avogadro's number,
 $\epsilon_p \Delta\Omega$ = photopeak efficiency of the NaI(Tl) crystal, including the solid angle effect

The factor

$$S(\mu, \langle L \rangle) = \frac{1 - e^{-\langle L \rangle \mu}}{\langle L \rangle \mu}$$

represents the fraction of γ -rays which escape the scattering sample⁽⁵⁾. The variation of this factor with the γ -ray energy, for some materials, is shown in Fig. 13.

The areas under the photopeaks have been deduced by means of a computer program⁽⁶⁾ and using the IBM 7044 computer of the "Centro di Calcolo dell'Università di Trieste".

The errors attached to the experimental points have been deduced taking into account the uncertainty

- a) in the total neutron counting (less than 1%),
- b) in the determination of the solid angle width (less than 2%),
- c) in the determination of the photopeak efficiency (3 ÷ 4%),
- d) in the determination of the photopeak area (from 5% to 20% according to the different intensities of the gamma lines).

All these errors have been taken as independent and quadratically added to give the mean experimental error.

The angular distributions of the 0.44 MeV and 1.63 MeV γ -rays from sodium are shown in Fig. 14.

It has to be noticed that the measured cross-sections refer to the total production of the observed γ -rays and do not represent the cross-section for the excitation of the nuclear levels since these can be excited either directly or through a cascade process from higher levels.

R e f e r e n c e s

- (¹) L. Granata and M. Lagonegro, Nucl. Instr. and Meth., 70 (1969) 93.
- (²) D.T. Stewart and P.W. Martin, Nucl. Phys. 60 (1964) 349.
- (³) U. Abbondanno, R. Giacomich,
L. Granata, M. Lagonegro and
G. Pauli, Report INFN/BE - 69/8
- (⁴) C.M. Davisson, in "Alpha-, Beta- and Gamma-Ray Spec-
troscopy", ed. by K. Siegbahn (North-
Holland Publishing Company, 1965),
Part I, Appendix I, p. 827.
- (⁵) F.C. Engesser and W.E. Thomp-
son, J. Nuclear Energy, 21 (1967) 487.
- (⁶) L. Vallon, Doctorate Thesis, University of Trie-
ste, 1970 (unpublished).

ACKNOWLEDGMENTS

The authors thank Prof. G. Poiani for his interest and encouragement in this work.

The authors wish also to thank S. Jasnig and G. Kidric for their valuable help in the design and construction of this apparatus, particularly with respect to the circuits described in this report, and the Centro di Calcolo dell'Università for assistance in the use of the computer program for the γ -spectra analysis.

The technical assistance of A. Lapel during the course of this work is also gratefully acknowledged.

Figure captions

- Fig. 1 - Schematic diagram of the experimental geometry.
- Fig. 2 - Schematic diagram of the electronics.
- Fig. 3 - Circuit diagram of the mixer unit.
- Fig. 4 - Circuit diagram of the tunnel diode discriminator of the gamma fast channels.
- Fig. 5 - Circuit diagram of the tunnel diode discriminators of the slow channels.
- Fig. 6 - Circuit diagram of the slow coincidence unit.
- Fig. 7 - Time-of-flight spectrum from sodium at a scattering angle of 60° . The time scale is ~ 0.4 nsec per channel.
- Fig. 8 - Circuit diagram of the preamplifier of the γ -channel for spectrometry.
- Fig. 9 - γ -ray spectrum from sodium at 60° .
- Fig. 10 - γ -ray spectrum from sodium at 120° .
- Fig. 11 - Photopeak efficiency of the NaI(Tl) crystals. With reference to figures 1 and 2, \bullet are related to the NaI(Tl) crystal N $^\circ$ 1, measuring at the angle ϑ , and \circ to the crystal N $^\circ$ 2, measuring at the angle $\pi - \vartheta$.
- Fig. 12 - Background spectrum taken with the sample removed at an angle of 60° .
- Fig. 13 - Fraction of γ -rays escaping the scattering sample as a function of γ -ray energy.
- Fig. 14 - Differential cross-sections for the 0.44 MeV (\circ) and 1.63 MeV (Δ) γ -rays from ^{23}Na . (Solid curves represent a best-fit with Legendre polynomials).

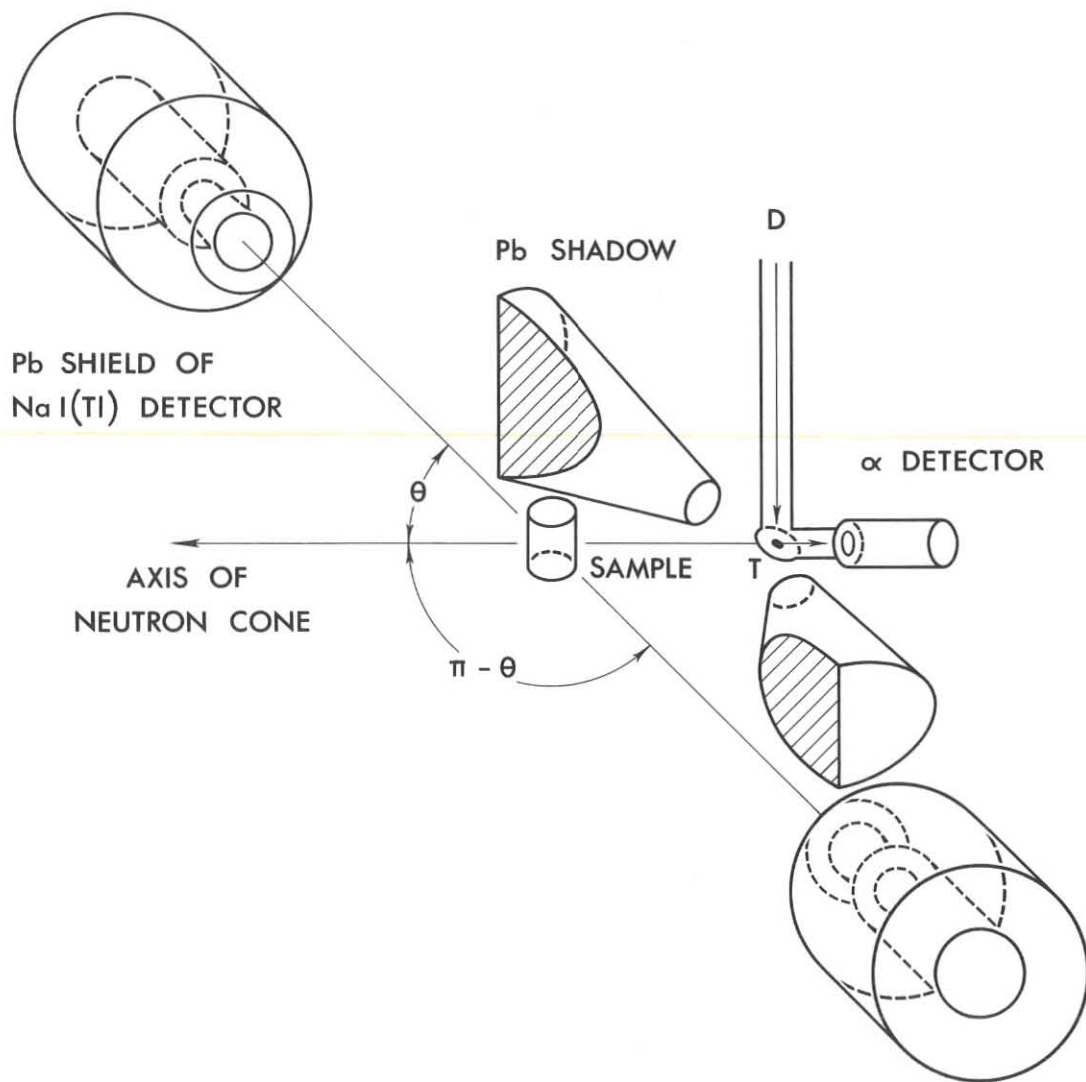


Fig. 1

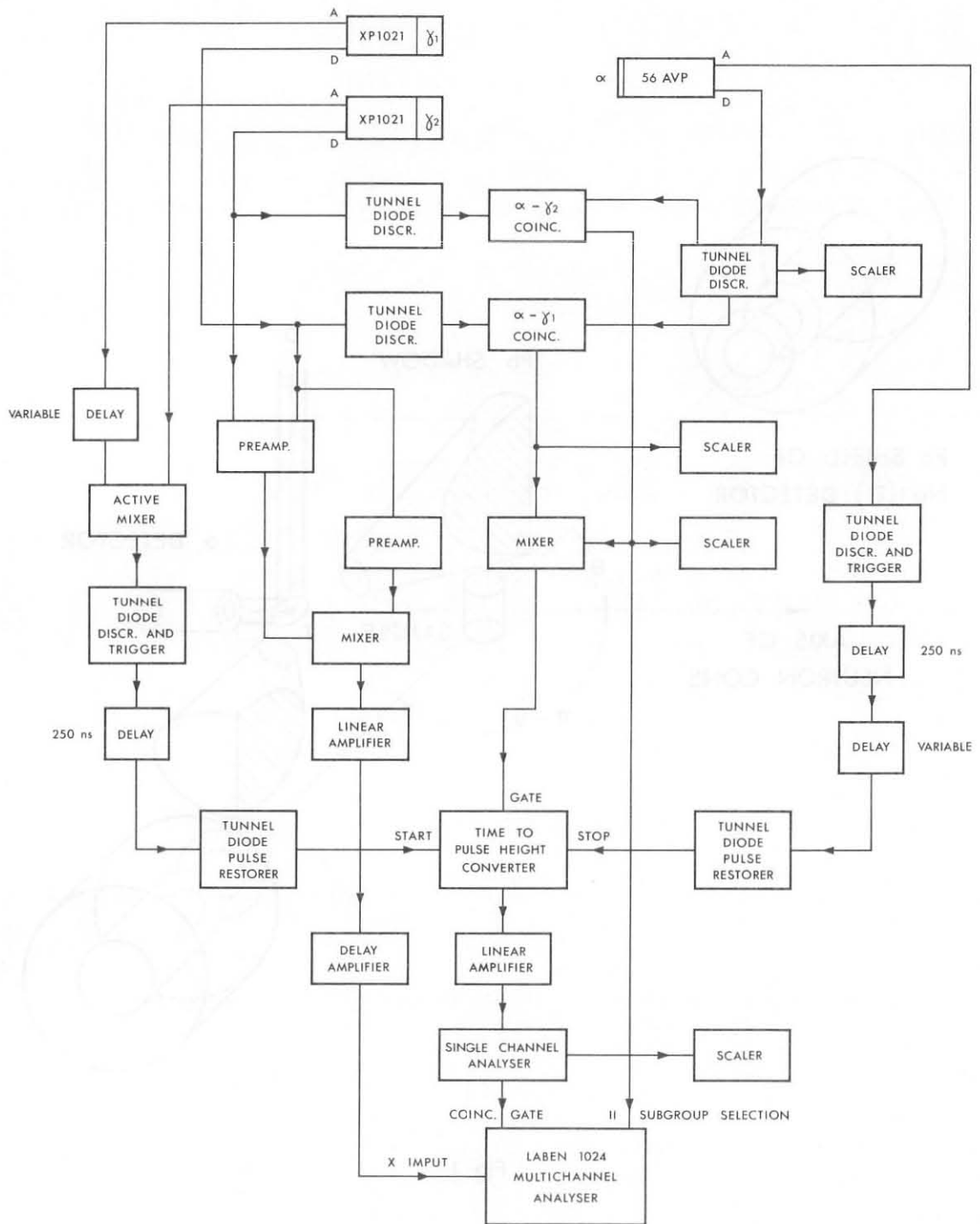


Fig. 2

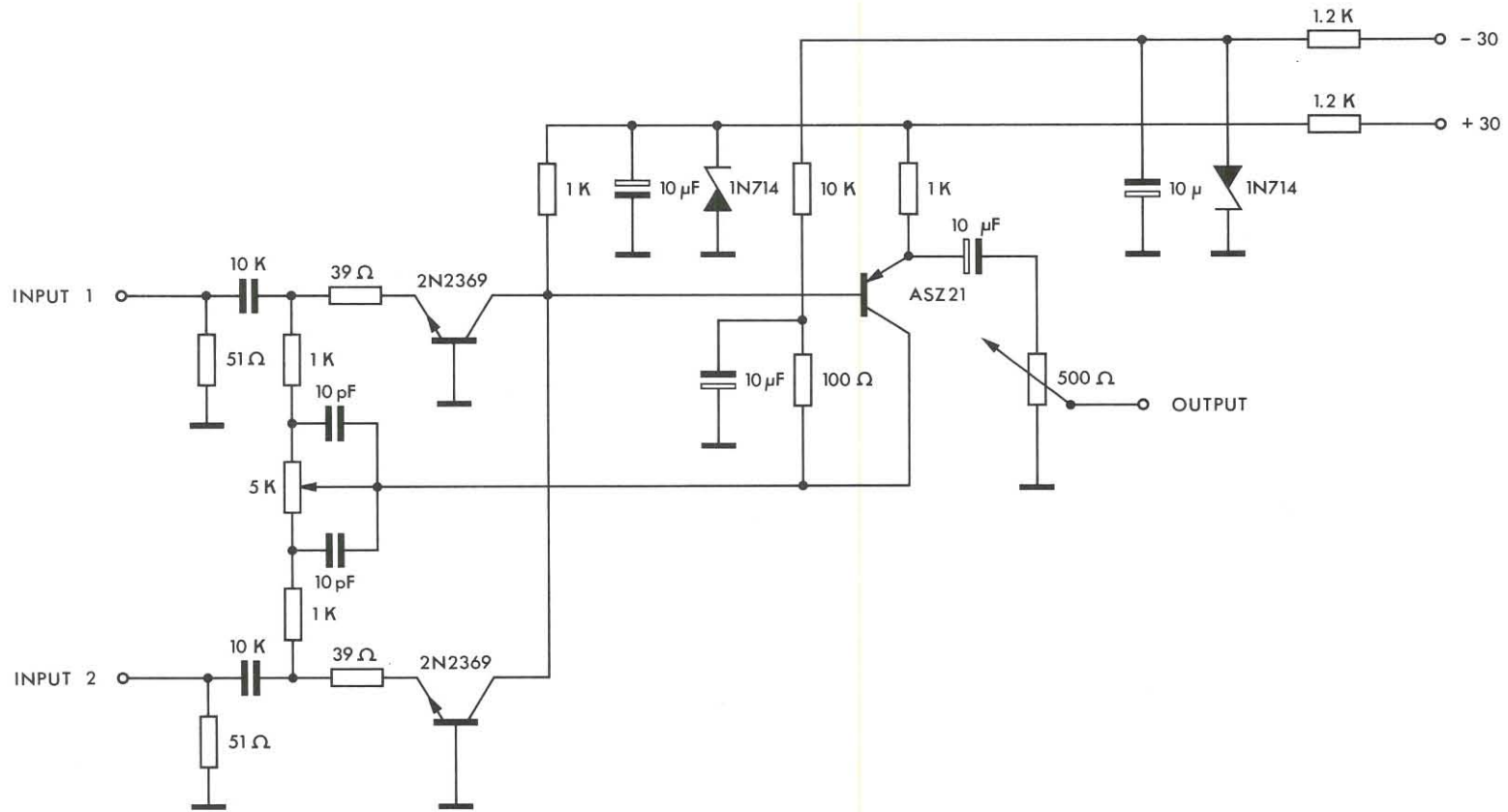


Fig. 3

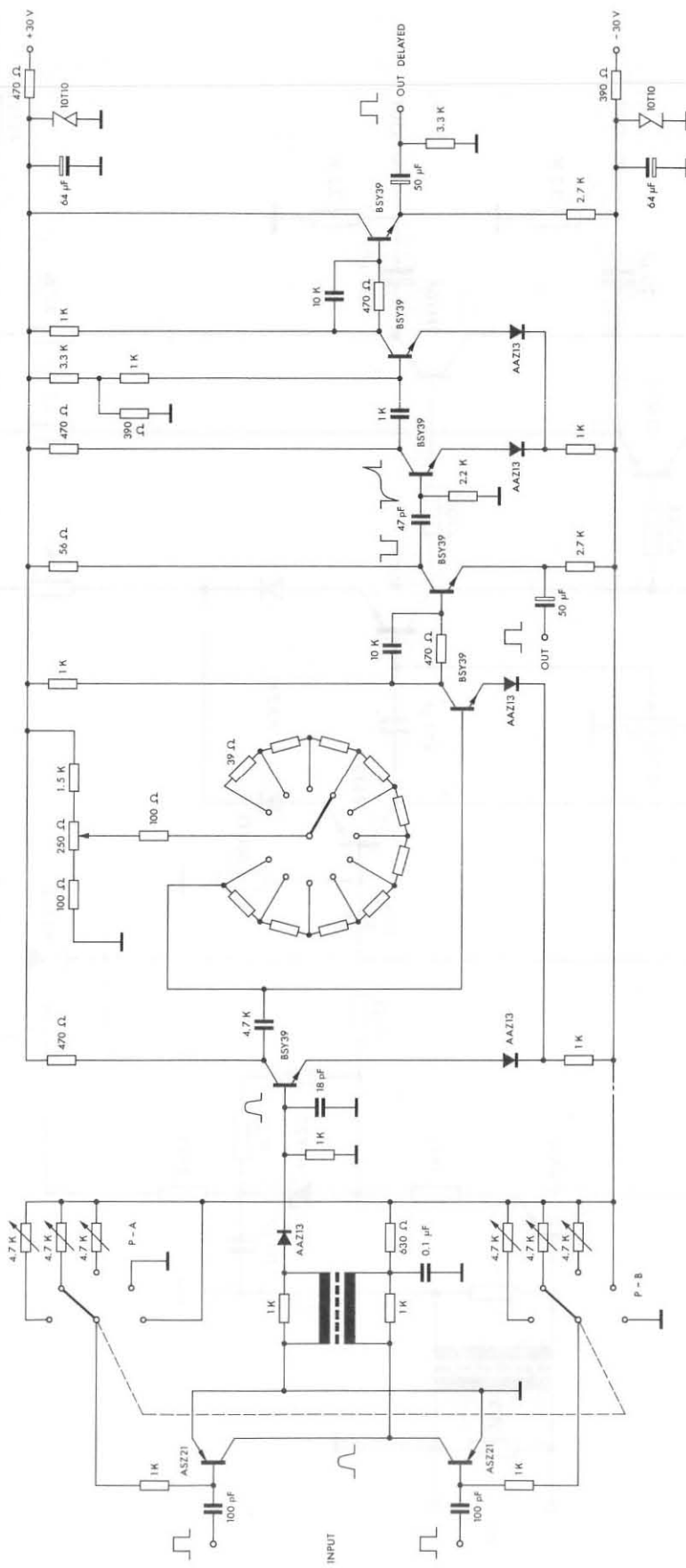


Fig. 6

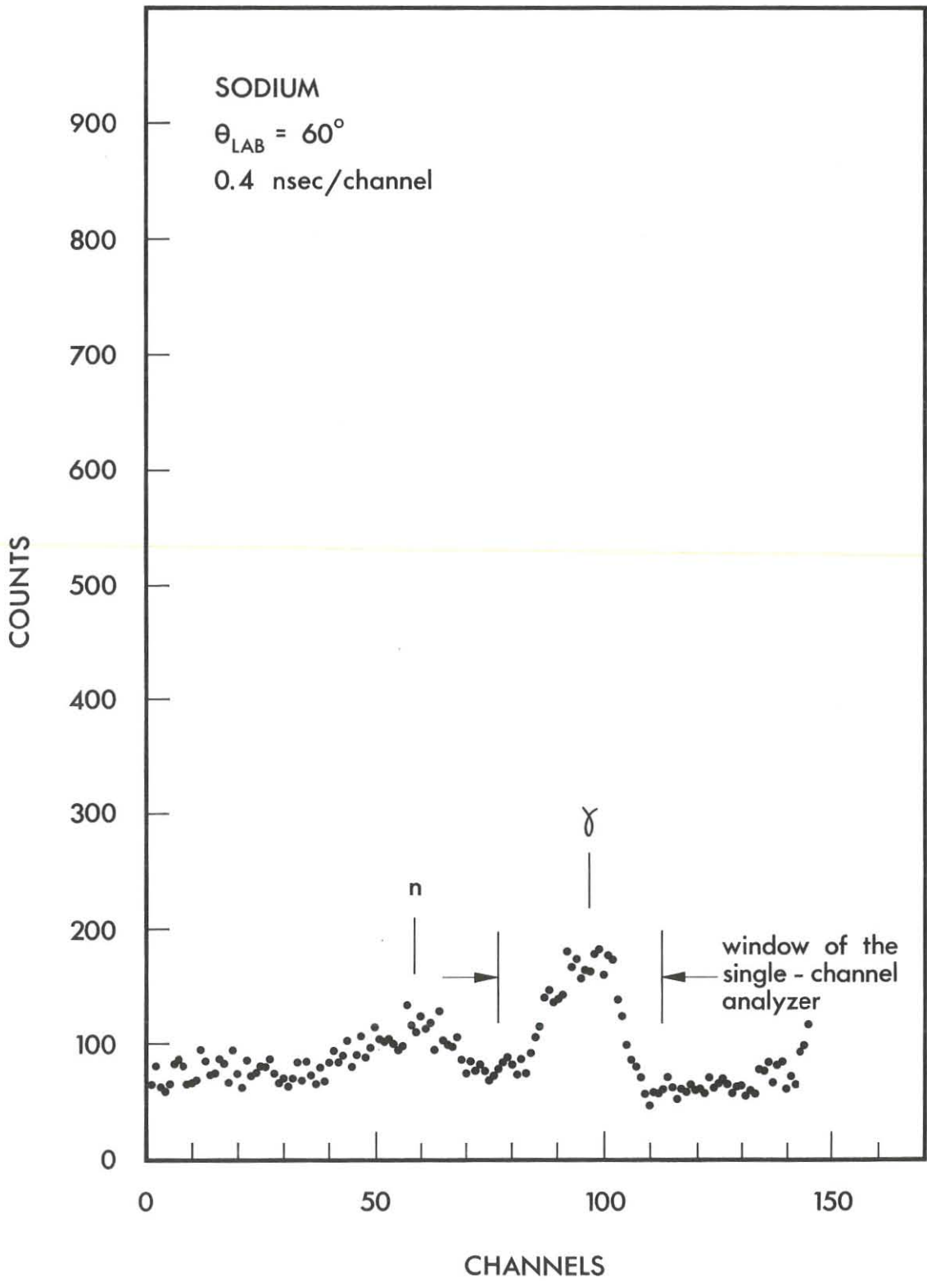


Fig. 7

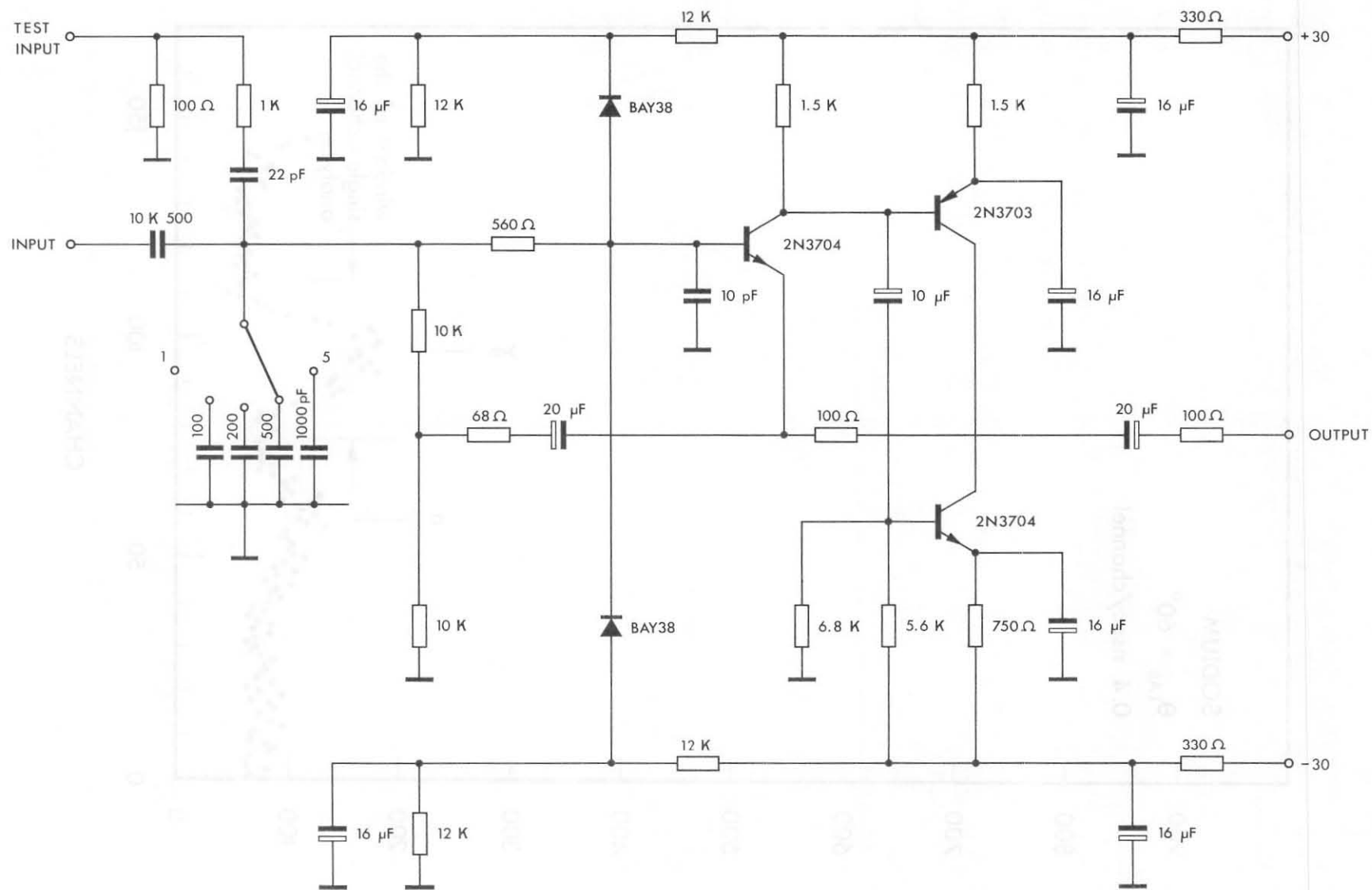


Fig. 8

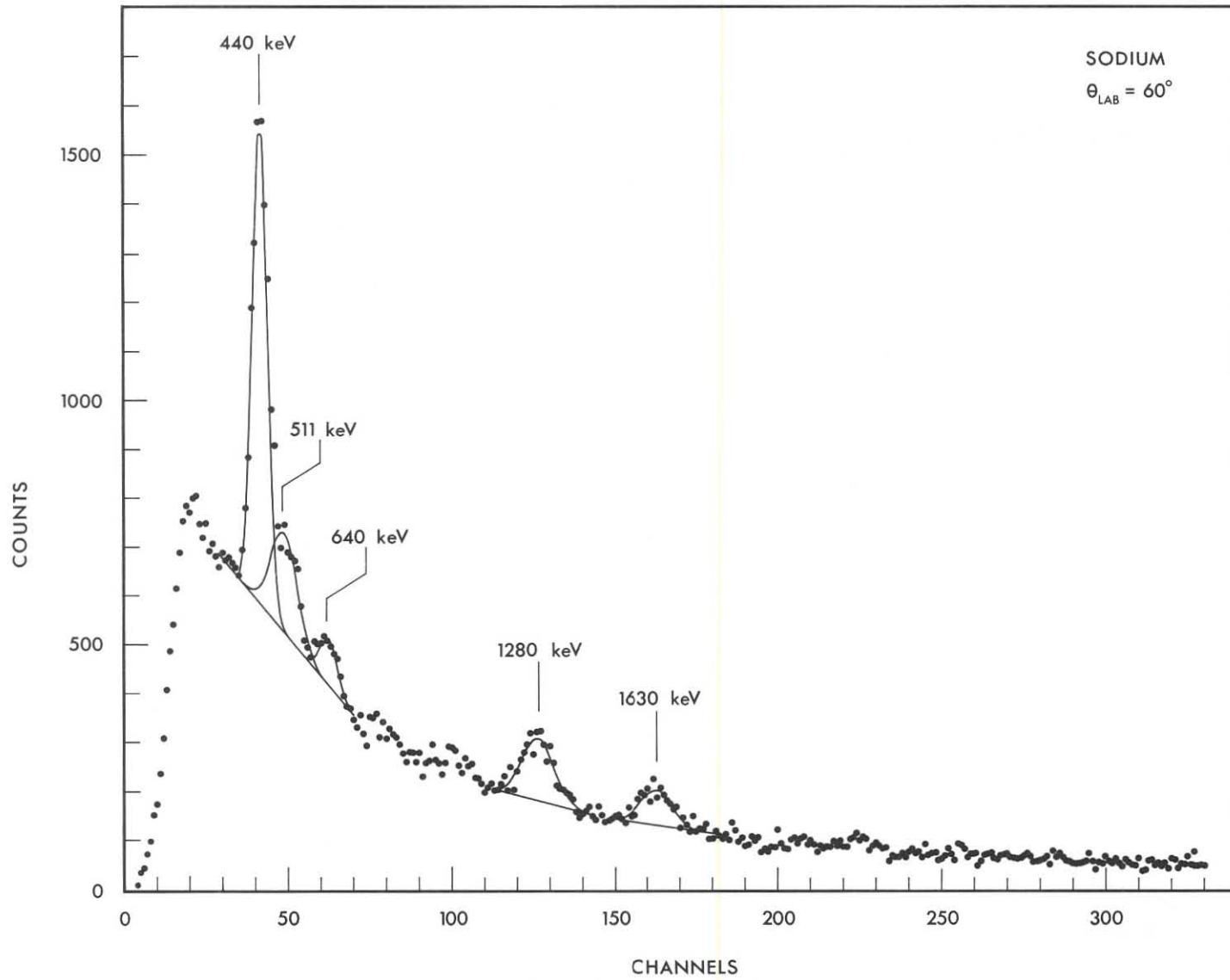


Fig. 9

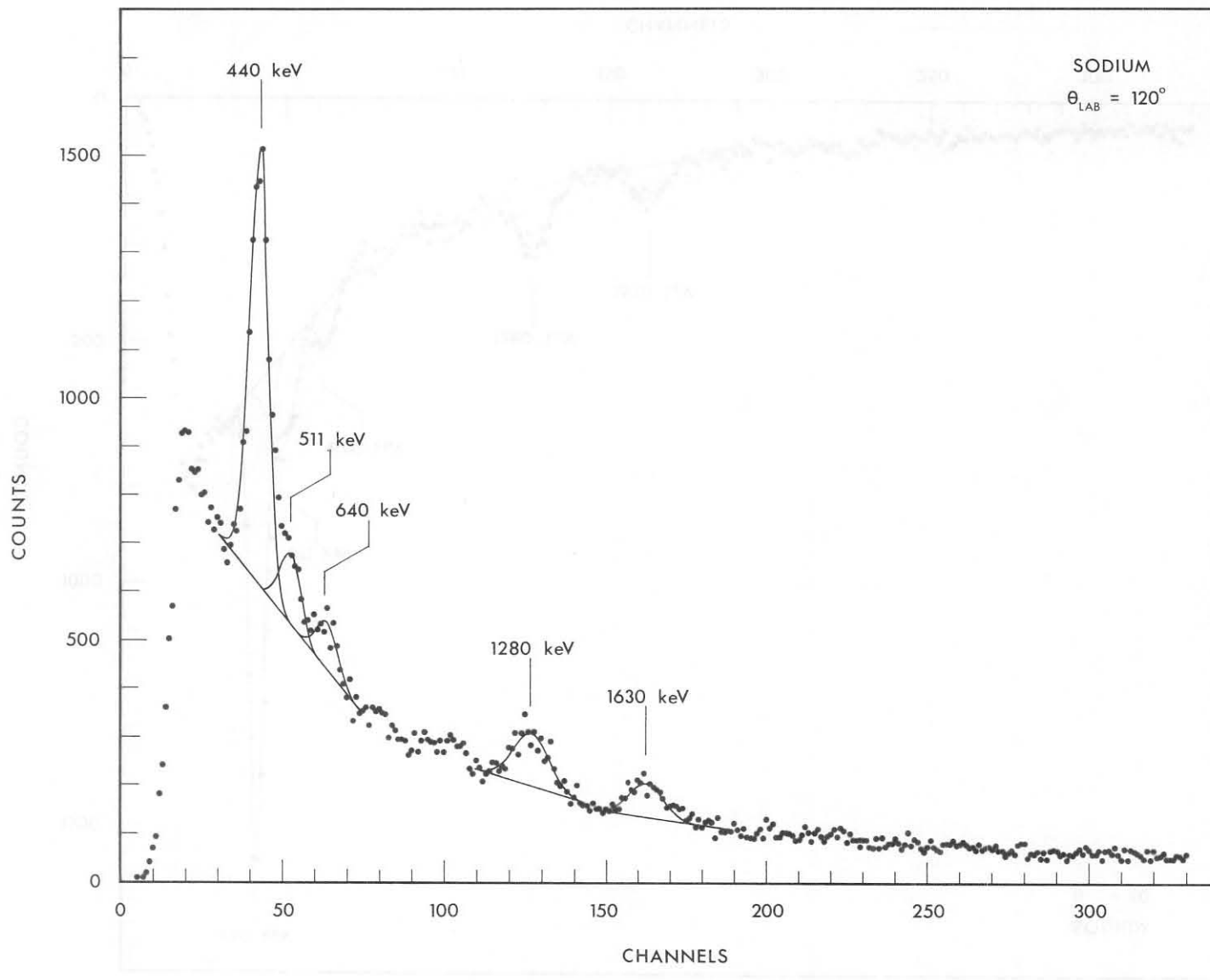


Fig. 10

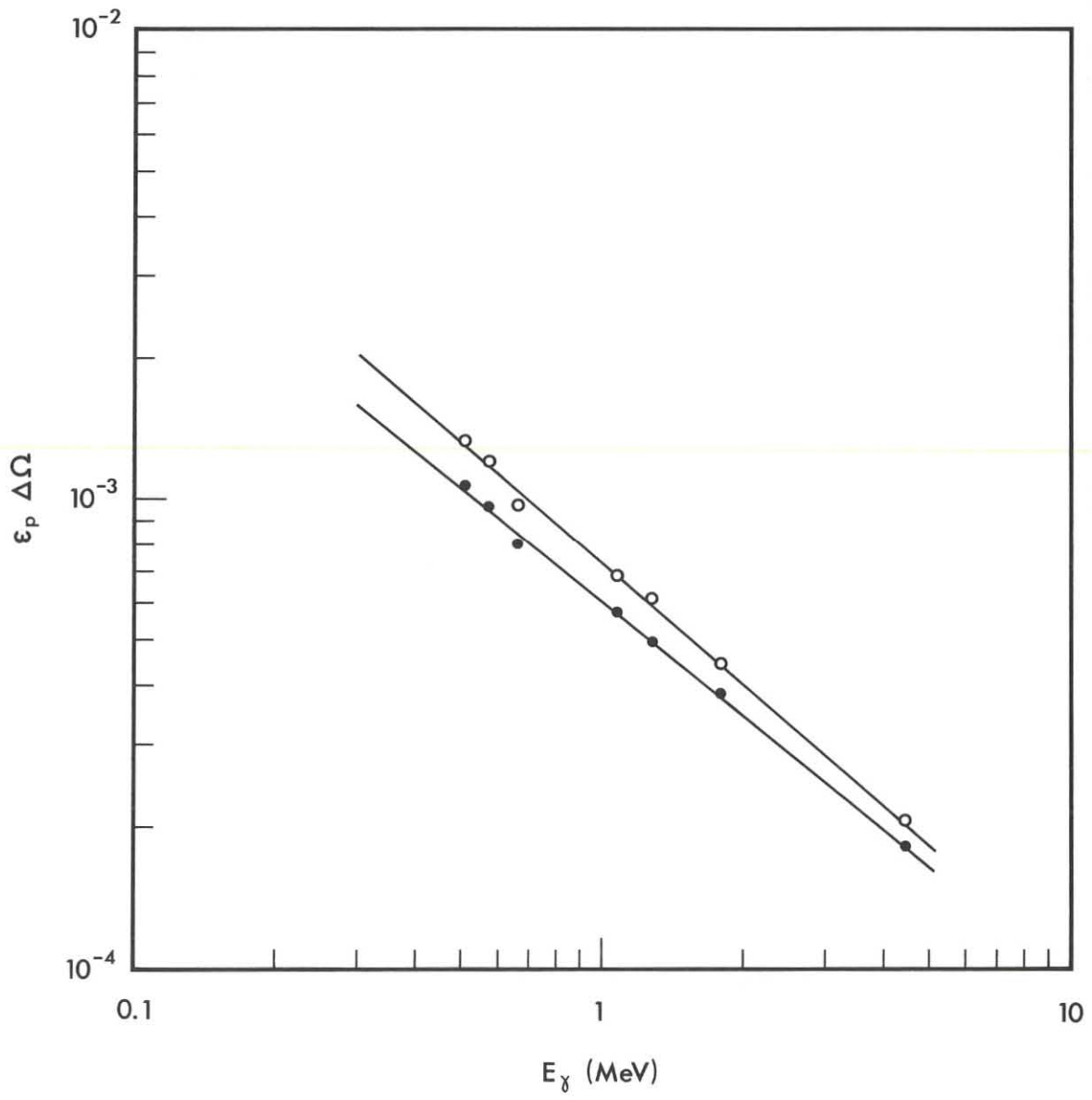


Fig. 11

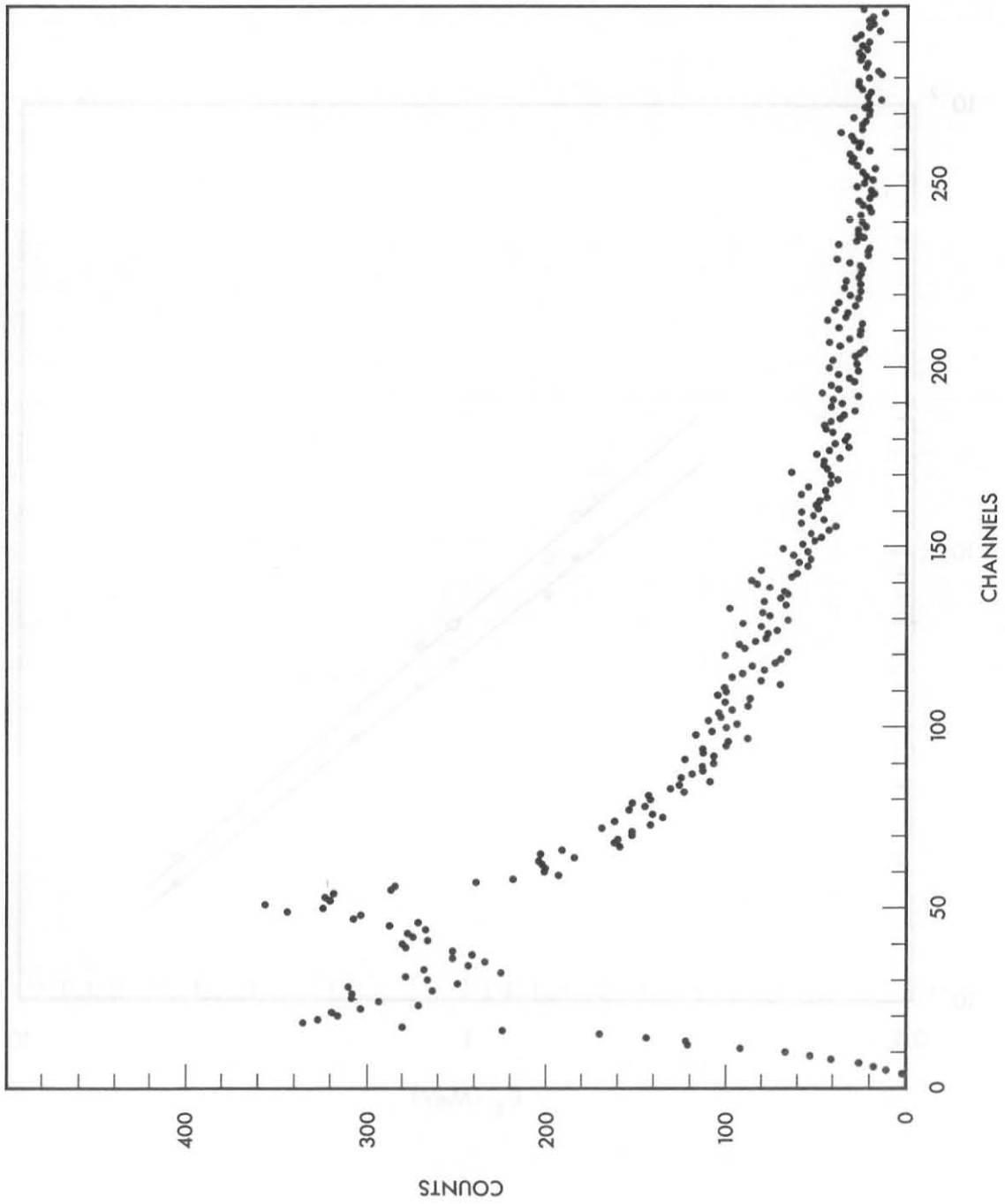


Fig. 12

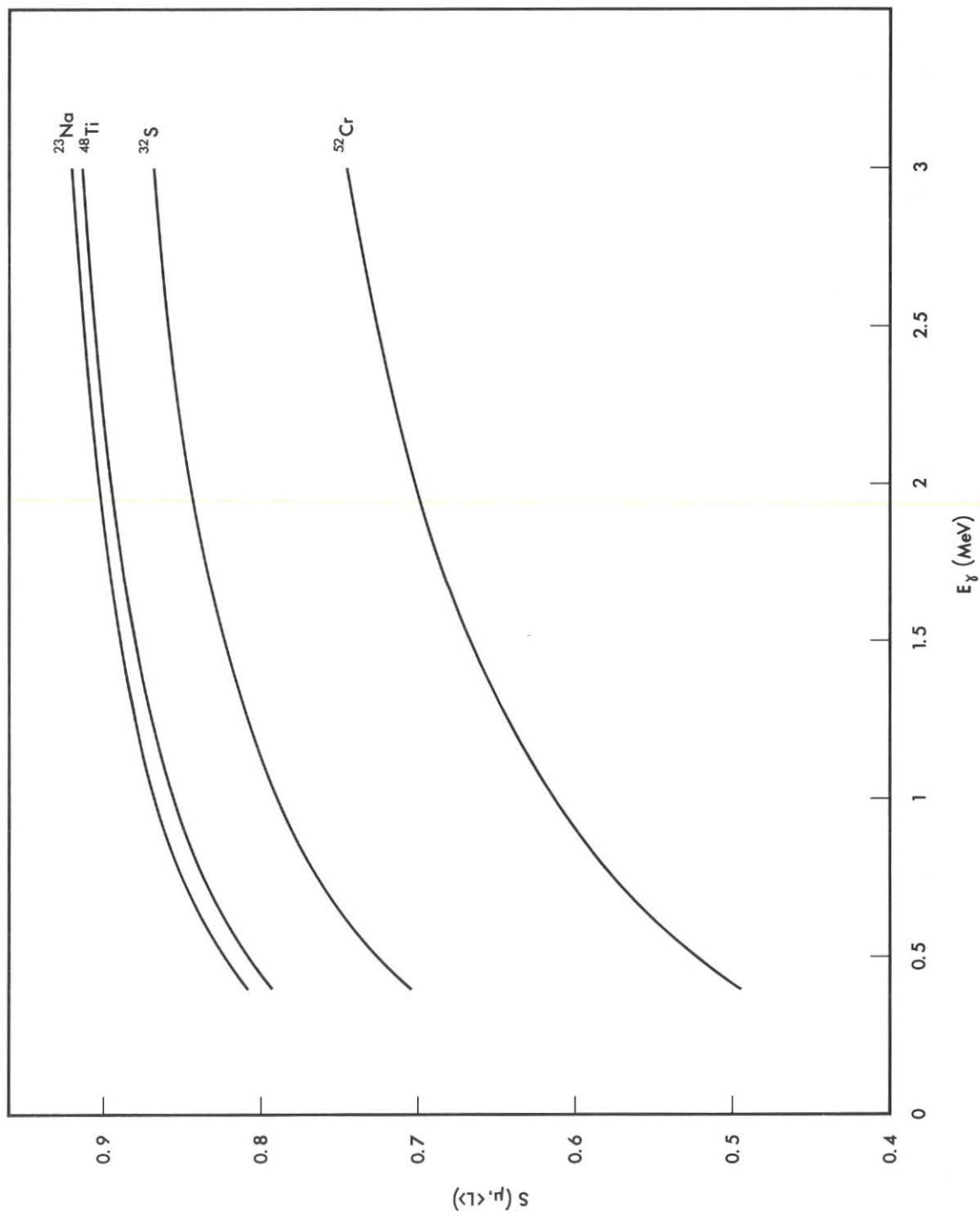


Fig. 13

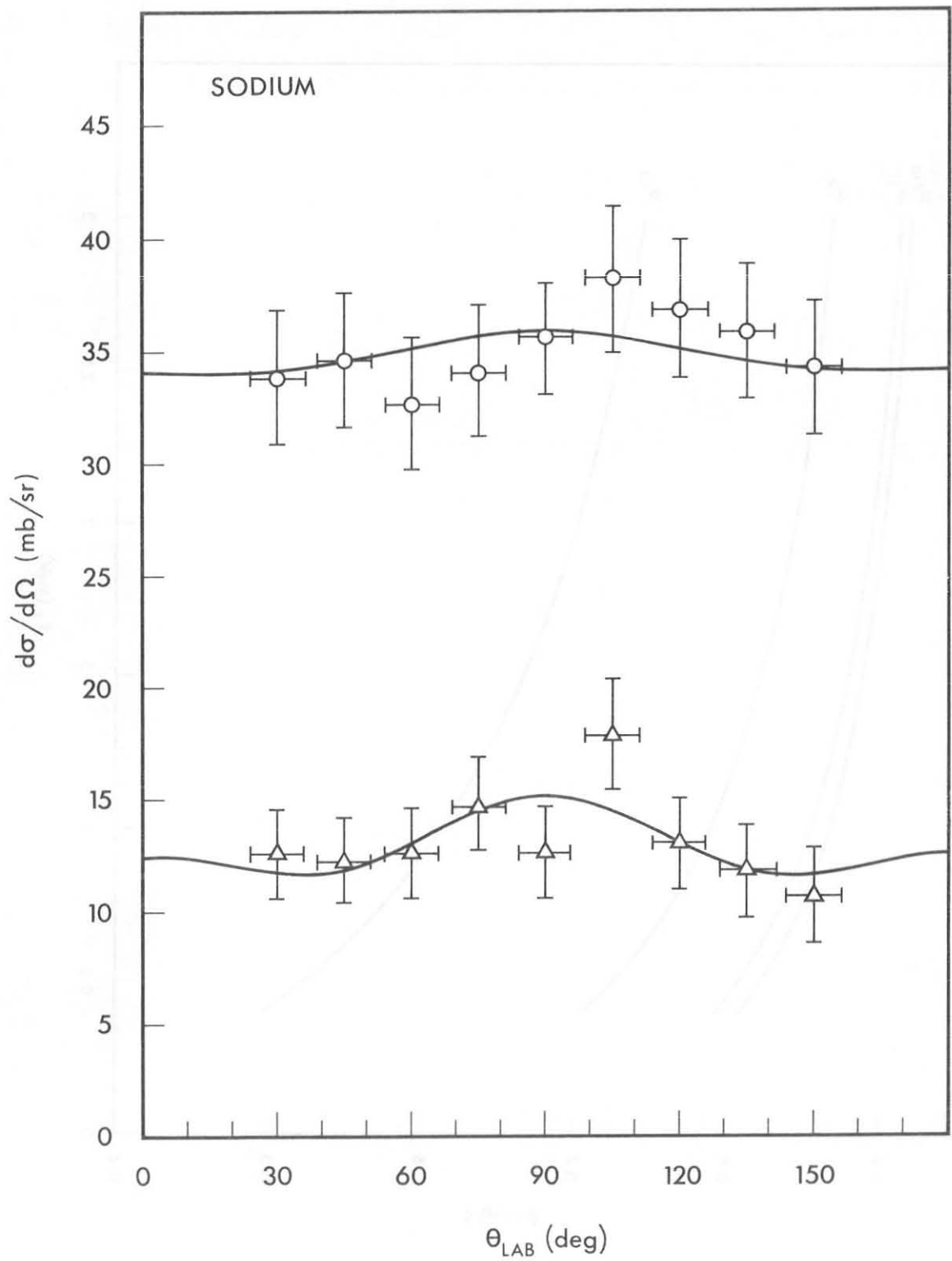


Fig. 14